Nuclear Instruments and Methods in Physics Research A 621 (2010) 247–257

Contents lists available at ScienceDirect

Nuclear Instruments and Methods in Physics Research A

journal homepage: www.elsevier.com/locate/nima

Implementation of the reverse/adjoint Monte Carlo method into Geant4

L. Desorgher [a,*], F. Lei [b], G. Santin [c]

[a] SpaceIT GmbH, Seftigenstrasse 115a, 3007 Bern, Switzerland
[b] Aerospace Division, QinetiQ, Farnborough GU14 OLX, UK
[c] Space Environments and Effects Section, European Space Agency/ ESTEC, Noordwijk 2200 AG, The Netherlands

ARTICLE INFO

Article history:
Received 18 December 2009
Received in revised form
31 May 2010
Accepted 1 June 2010
Available online 9 June 2010

Keywords:
Adjoint Monte Carlo
Geant4
Radiation shielding

ABSTRACT

We have implemented the reverse/adjoint Monte Carlo method into Geant4. In this method the primary particles are tracked backward from the sensitive part of the geometry till the external source surface by following the reverse processes. By this way the computing time is spent only for tracks that are contributing to the tallies and the reverse Monte Carlo method is much more rapid than the normal forward Monte Carlo method for simulation cases where the sensitive part is small compared to the rest of the geometry and compared to the extended external source. In this paper we first present the theoretical principles of the Reverse Monte Carlo method. Then we describe how this method and the reverse processes have been implemented into Geant4. Finally we compare and discuss the simulation results obtained with the reverse and forward Monte Carlo modes in Geant4.

1. Introduction

The Monte Carlo (MC) method is probably the most accurate approach for simulating the interaction of radiation within complex geometries. However, in most cases MC simulations need a lot of computing time in order to reach the desired precision of the simulation results. When the sensitive part of a detector is significantly small compared to its entire size and to the size of the external extended particle source, a lot of computing time is spent in the simulation of particle showers that are not contributing to the detector signal. This is typically the case in the space dosimetry calculations where only the doses in tiny specific components of a spacecraft or instrument electronics are required. In such cases the reverse Monte Carlo (RMC) method, also known as the adjoint Monte Carlo method, can be used to speed up the calculations. In this method the primary particles are generated in the sensitive volume of the instrument and are then tracked backward in the geometry until they reach the external source surface, or exceed an energy threshold. Reverse Monte Carlo techniques have first been applied with success in the sixties by nuclear scientists to obtain a fast evaluation of the radiation dose on some part of nuclear reactors [1,2]. The adjoint Monte Carlo method is also available in the NOVICE code which is used widely by the space industry for radiation analysis of space systems [3].

Recently we have implemented the RMC method into Geant4 [4] for the e^-, proton and ion continuous and discrete ionization, multiple scattering, e^- bremsstrahlung, photo-electric effect, and Compton scattering processes. In this paper we describe in Section 2 the theoretical principles of the reverse/adjoint MC method. In Section 3 the way we have implemented the RMC method in the Geant4 toolkit is presented. The update of the Geant4 Radiation Analysis for Space tool (GRAS), developed at the European Space Agency (ESA) [5] is briefly described in Section 4 as an example of application code making use of the newly developed Geant4 RMC classes. Results of Geant4 GRAS reverse and forward MC simulations are compared and discussed in Section 5. Finally conclusions are presented in Section 6.

2. Theoretical principles of the reverse Monte Carlo method

Different theoretical approaches of the RMC method have been proposed in the scientific literature [2,6,7,1,8,9]. In general the adjoint transport equation describing the reverse treatment of a problem is transformed to make it look like a forward transport equation, allowing the identification of the transport kernel, the collision kernel, the weight correction procedure, and the normalization procedure that have to be considered in the reverse case. In this paper we present the RMC method in a more direct way, closer to the treatment presented in Jordan [9]. We consider the simulation case illustrated in Fig. 1 where the current of secondary particles, induced by the interaction of an external source of particles (big circle) with the geometry of the problem, is computed on a given surface (small circle). In the forward MC treatment the primary particles are generated randomly on the external source surface and tracked in the geometry. The resulting scattered primaries and

* Corresponding author. Tel.: +41 313014080.
E-mail address: desorgher@spaceit.ch (L. Desorgher).

0168-9002/$ - see front matter © 2010 Elsevier B.V. All rights reserved.
doi:10.1016/j.nima.2010.06.001

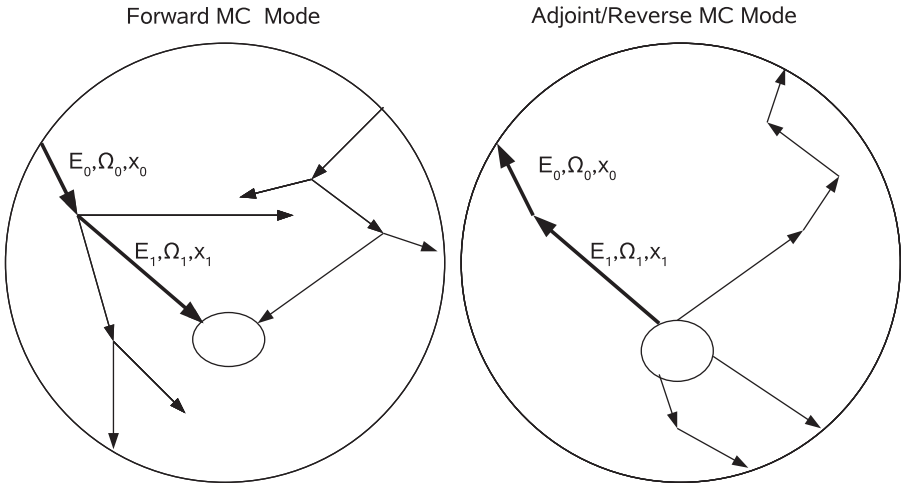

Fig. 1. Schematic view of the forward and reverse Monte Carlo integration methods. In the forward MC method primary particles are generated randomly on the external surface (big circle) and tracked randomly in the geometry. Only a limited part of the tracks reach the sensitive region (delimited by the small circle) where signals are registered. In the reverse Monte Carlo mode primary adjoint particles are generated on the boundary of or in the sensitive region and are tracked backward till the external surface with reverse processes acting on the particles. By this way the computing time is reserved only to tracks that are contributing to the detector signals.

secondaries are registered on the detecting surface. In this case a primary particle is the source of different secondary tracks and all these tracks are sampled randomly by considering the cross-sections of the different processes that they undergo (ionization, bremsstrahlung, etc.). In the reverse treatment of the problem the so-called primary adjoint particles are generated on the detection surface and tracked backward in the geometry with reverse reactions taken into account. In a reverse reaction an adjoint projectile is equivalent to one of the products or the scattered projectile of the corresponding forward reaction and is changed in an adjoint secondary that is equivalent to the forward projectile. Therefore in the reverse world a forward process is split into different reactions which are the scattered projectile to projectile reaction and the product to projectile reactions.

To present the theoretical principles of the RMC method we consider how the track painted in bold in Fig. 1 would be treated in both the forward and reverse MC modes. It corresponds to the case where a source particle of type i of energy E_0 and direction Ω_0, travels over a distance x_0 before interacting with an atom A of the geometry. The products of this interaction are the scattered primary plus two secondaries. The second secondary of type j has an energy E_1 and direction Ω_1, it travels without interaction over x_1 before hitting the detecting surface.

2.1. Forward Monte Carlo integration

In the forward MC mode the probability for a primary particle of type i to travel freely over x_0 and then interact over a distance dx on an atom A with the production of a secondary of type j with energy E_1 and direction Ω_1 is given by

$$e^{-\int_0^{x_0}\Sigma_{i,t}(E_0,x)\,dx}N_A\frac{\partial^2\sigma(E_0)}{\partial E_1\partial\Omega}\,dx\,dE_1\,d\Omega_1 \tag{1}$$

with $\Sigma_{i,t}(E_0,x)$ the total macroscopic cross-section for the particle of type i, $\partial^2\sigma/\partial E_1\partial\Omega$ the double differential microscopic cross-section of the reaction that occurs, and N_A the atomic density of the atom of type A at the position of the interaction. For the second step of the bold track (Fig. 1), the probability that the secondary of type j travels in the geometry over a distance x_1 without interaction is given by

$$e^{-\int_0^{x_1}\Sigma_{j,t}(E_1,x)\,dx} \tag{2}$$

with $\Sigma_{j,t}(E_1,x)$ being the total macroscopic cross-section for the secondary particle of type j. Considering Eqs. (1) and (2) the normalized weight of the bold track is then given by

$$W = W_s e^{-\int_0^{x_0}\Sigma_{i,t}(E_0,x)\,dx}N_A\frac{\partial^2\sigma(E_0)}{\partial E_1\partial\Omega}\,dx\,dE_1\,d\Omega_1 e^{-\int_0^{x_1}\Sigma_{j,t}(E_1,x)\,dx}. \tag{3}$$

The factor W_s in this equation represents the weight of the primary particle in the source and is given by

$$W_s = f(E_0,\Omega_0)\,dE_0\,d\Omega_0\cos\theta_s\,dS_s \tag{4}$$

with $f(E_0,\Omega_0)$ the differential directional flux of the primary source, dS_s the infinitesimal surface element on the source from which the primary particle is emitted, and θ_s the angle between the normal to the surface element and the particle direction Ω_0. The Monte Carlo sampling of a big enough number of forward tracks is equivalent to the integration of the weight W over all independent variables $(E_0,\Omega_0,S_s,x_0,E_1,\ldots)$ appearing in the tracks, summed over all type of reactions, atomic elements, primaries, and secondaries. In this integration the cases where more than one reaction and no reaction occur are also considered but only the tracks reaching the sensitive surface are accounted for.

2.2. Reverse Monte Carlo integration

2.2.1. Adjoint cross-sections

In the reverse Monte Carlo method for each scattered primary and each product of a forward reaction a separate corresponding reverse reaction is considered. The adjoint differential cross-section $\partial^2\sigma^+(E)/\partial E'\partial\Omega$ that is used for the sampling of a given reverse reaction is equivalent to the differential cross-section used in the forward case but with projectile and product (or scattered projectile) energy being inverted. In other words we have

$$\frac{\partial^2\sigma^+(E)}{\partial E'\partial\Omega} = \frac{\partial^2\sigma(E')}{\partial E\partial\Omega} \tag{5}$$

with $\partial^2\sigma(E')/\partial E\partial\Omega$ the differential cross-section of the forward reaction, and Ω giving the direction of the product or scattered projectile relative to the projectile direction. The adjoint microscopic cross-section associated with a reverse reaction is obtained by the integration of the differential adjoint cross-section over the energy and direction of the adjoint secondary equivalent to the

forward projectile. It writes

$$\sigma^+(E) = \int\int \frac{\partial^2\sigma^+(E)}{\partial E'\partial\Omega}\,dE'\,d\Omega = \int\int \frac{\partial^2\sigma(E')}{\partial E\partial\Omega}\,dE'\,d\Omega. \quad (6)$$

Finally the total adjoint macroscopic cross-section $\Sigma^+_{i,t}(E)$ for a specific type of particle i and a given material is obtained by summing all the adjoint microscopic cross-sections over all types of reverse reactions where the particle of type i is involved as adjoint projectile, and over all elements of the material, weighted with the atomic densities.

The same method used in the forward case is then applied for the random sampling of the reverse tracks and reverse reactions but using the adjoint cross-sections instead of the forward ones. By this way in the reverse method, without considering other biasing and weight corrections, the bold track in Fig. 1 will be associated with the following weight:

$$W = W_d e^{-\int_0^{x_1}\Sigma^+_{j,t}(E_1,x)\,dx} N_A \frac{\partial^2\sigma(E_0)}{\partial E_1\partial\Omega}\,dx\,dE_0 d\Omega_0 e^{-\int_0^{x_0}\Sigma^+_{i,t}(E_0,x)\,dx} W_n \quad (7)$$

with W_d associated with the sampling of the adjoint primaries on the detection surface and the W_n the factor of normalization to the external flux. By comparing Eqs. (3) and (7), it is clear that additional weight corrections and normalization factors have to be applied to the reverse tracks in order to get weights equivalent to the forward case.

2.2.2. Sampling and weight of the adjoint primaries

The adjoint primary particles are randomly sampled with a uniform position distribution on the detection surface, with an outward direction generated from a cosine law distribution relative to the surface normal, and with a spectrum $I(E)$. In order to reduce the variance of the reverse MC tracking the spectrum $I(E)$ is set different than a flat spectrum. A minimum variance of the reverse MC integration would be obtained if $I(E)$ would be set to the spectrum of the secondary particles on the detection surface obtained in the forward problem. However, as this solution is clearly not known, $I(E)$ is usually set to a $1/E$ spectrum.

The way the primary adjoint particles are generated implies that the weight W_d in Eq. (7) writes

$$\begin{aligned} W_d &= n\frac{I(E_1)\,dE_1}{\int_{E_{min}}^{E_{max}} I(E)\,dE}\frac{\cos\theta_d\,d\Omega_1}{2\pi\int_0^{\pi}\cos\theta\sin\theta\,d\theta}\frac{dS_d}{\int_{A_d} dS_d} W_{prim} \\ &= n\frac{dE_1}{E_1\log\frac{E_{max}}{E_{min}}}\frac{\cos\theta_d\,d\Omega_1}{\pi}\frac{dS_d}{A_d} W_{prim} \end{aligned} \quad (8)$$

with n the number of adjoint primaries generated, E_{min} and E_{max} the minimum and maximum energy of the adjoint primaries, dS_d the infinitesimal element of the detection surface, θ_d the angle between the normal to the surface element and the particle direction Ω_1, A_d the area of the entire surface, and W_{prim} the weight of the primary adjoint particle. The weight of an adjoint primary particle W_{prim} is set to

$$W_{prim} = \frac{\pi A_d\int_{E_{min}}^{E_{max}} I(E)\,dE}{n_{prim} I(E_1)} = \frac{\pi A_d E_1 \log\frac{E_{max}}{E_{min}}}{n} \quad (9)$$

in order to get

$$W_d = dE_1\,d\Omega_1\,dS_d\cos\theta_d. \quad (10)$$

2.2.3. Weight correction factors

The fact that in the RMC mode adjoint total cross-sections are used instead of the forward ones to sample the distance to the next reaction implies that the probability of a particle to survive over a distance x is $e^{-\int_0^x \Sigma^+_t(E,x)\,dx}$ instead of $e^{-\int_0^x \Sigma_t(E,x)\,dx}$. In order to correct for this difference two solutions can be applied. In the first one the weight of an adjoint particle after a step is multiplied by the factor

$$W_{step} = e^{-\int_0^x \Sigma_t(E,x)\,dx} / e^{-\int_0^x \Sigma^+_t(E,x)\,dx}. \quad (11)$$

In this case as the adjoint differential cross-sections are equivalent to the forward ones no correction factor is needed after the sampling of the reverse reaction products. The other solution is to scale all the differential adjoint cross-sections by the same factor $f = \Sigma_t(E,x)/\Sigma^+_t(E,x)$ such that the total cross-sections used in both the reverse and forward cases are equal. In this case the correction factor $W_{step}=1$ and is not necessary anymore, but a weight correction factor

$$W_{react} = \frac{\Sigma^+_t(E)}{\Sigma_t(E)} \quad (12)$$

is applied to the adjoint secondary or scattered primary of a reverse reaction, since the adjoint and forward differential cross-sections are now different by the factor $\Sigma_t(E)/\Sigma^+_t(E)$.

2.2.4. Additional biasing of the differential cross-sections

Biasing of the differential adjoint cross-sections can be applied for different reasons e.g. to increase the occurrence of a specific process, to use a simple analytical approximation of the differential cross-section of a reverse reaction to have a rapid sampling of the secondaries, or to limit the variance of the reverse MC tracking. Any of these biasings has to be corrected after the occurrence of a reverse reaction by multiplying the weight of the secondary by the factor

$$W_{dCS} = \frac{\partial^2\sigma(E)}{\partial E'\partial\Omega}\Big/\frac{\partial^2\sigma_{bias}(E)}{\partial E'\partial\Omega} \quad (13)$$

representing the ratio between the correct differential cross-section $\partial^2\sigma(E)/\partial E'\partial\Omega$ and the biased differential cross-section $\partial^2\sigma_{bias}(E)/\partial E'\partial\Omega$.

As already mentioned in Section 2.2.2, the primary adjoint particles are generated with a spectrum $I(E)$ different than a flat spectrum in order to reduce the variance of the reverse MC tracking. For the same reason the adjoint differential cross-sections are multiplied by a factor $I(E')/I(E)$ with E and E' the energies of the adjoint projectile and product, respectively. This additional biasing implies the following weight correction factor:

$$W_{bias} = \frac{I(E)}{I(E')} = E'/E \quad (14)$$

to the product of a reverse reaction.

2.2.5. Normalization to the external source and final weight

The normalization to the external flux is done by multiplying the weight of the adjoint particles reaching the external source surface by their corresponding directional flux. So finally by considering all the normalization and weighting factors explained above, the weight of the reverse tracks when reaching the external surface writes

$$\begin{aligned} W = {} & dE_1\,d\Omega_1\cos\theta_d\,dS_d e^{-\int_0^{x_1}\Sigma_{j,t}(E_1,x)\,dx} N_A \\ & \times\frac{\partial^2\sigma(E_0)}{\partial E_1\partial\Omega}\,dx\,dE_0\,d\Omega_0 e^{-\int_0^{x_0}\Sigma_{i,t}(E_0,x)\,dx} f(E_0,\Omega_0). \end{aligned} \quad (15)$$

The only remaining difference between this weight and the forward weight in Eq. (3) comes from the factors $\cos\theta_d\,dS_d$ and $\cos\theta_s\,dS_s$. They represent the area of the section of the flux tubes, associated with the bold track (Fig. 1), on the detecting surface and on the external surface, respectively. The area of a flux tube being conserved along a track, $\cos\theta_d\,dS_d$ and $\cos\theta_s\,dS_s$ are the same

and finally the weight in Eqs. (3) and (15) are equal. The Monte Carlo sampling of a big enough number of reverse tracks is equivalent to the integration of the weight W over all independent variable $(E_1,\Omega_1,S_d,x_1,E_0,\ldots)$ summed over all type of reverse reactions, atomic elements, adjoint primaries, and adjoint secondaries. In this integration the cases where more than one reaction and no reaction occur are also considered and only the tracks reaching the external source are accounted for. By this way the same answer is obtained as in the forward case.

2.2.6. Weight correction for continuous energy gain

In both forward and reverse MC methods that we have described above we did not consider the continuous loss of energy of charged particles. This continuous energy change is treated in the reverse case by a continuous gain of energy over a tracking step. This implies that an extra weight correction is required. Indeed in the reverse MC integration the weight in Eq. (15) is integrated over the energy of the adjoint particles directly after their production either on the detection source or from a reverse reaction, while to match the forward case it should be integrated over their energy just before a reverse reaction occurs corresponding to the time when they are produced in the forward case. When no continuous gain of energy is considered the energy is kept constant over a step and the forward and reverse MC integrations are then equivalent as we have seen above. However, when the continuous gain of energy is taken into account a contraction or dilatation of the energy distribution take place and dE gets smaller or higher over a step. To integrate the weight over the energy of the adjoint particle at the end of steps rather than at the beginning of step, the different dE in Eq. (15) have to be replaced by their values dE' at the end of steps. This is done by correcting the weight of adjoint particles after each step by the factor

$$W_{dE}=\frac{dE'}{dE}=\frac{dE'/dx}{dE/dx} \tag{16}$$

representing the ratio between the stopping power of the adjoint particles after and before a tracking step.

3. Implementation of the reverse MC method in Geant4

We have implemented the reverse MC method into Geant4 for the electromagnetic physics of e^-, proton, and ions.

3.1. Main design

The way we have implemented the reverse MC method in Geant4 is illustrated in Fig. 2. A reverse MC simulation in Geant4 is a succession of reverse (black) and forward tracking (grey) starting in opposite directions from a surface containing the sensitive part of the detector. This surface, represented by the small circle in Fig. 2, is referred as the adjoint source. During the reverse tracking the weight of a secondary particle on the adjoint surface, that would result from the interaction with the geometry of a particle starting on the external sphere, is computed applying the RMC method described above. In the forward phase a forward Geant4 tracking event is used to compute the signal induced by the particle entering the sensitive part of the geometry from the adjoint source.

In more details, adjoint particles corresponding to forward ones (adjoint e^-, γ, protons, etc.) are generated one by one randomly on the adjoint source with a biased spectrum $I(E)=1/E$, and their weight set to the value given in Eq. (9). The adjoint source can be set by the user either to the surface of a sensitive volume in the geometry or on a sphere containing sensitive volumes. The uniform position distribution over the adjoint surface and the cosine law distribution of the direction relative to the primary surface is obtained for any kind of convex volume by ray-tracing technique. The same technique is used to compute the area of the adjoint source A_d in Eq. (9). All types of primary and secondary particles encountered in the forward simulation are considered as adjoint primaries in order to cover all possible types of secondary that could arrive on the boundary of the sensitive part of the geometry. After its generation on the adjoint source surface the primary adjoint particle is tracked backward in the geometry, applying the reverse reaction processes, and its weight is changed according to the formula explained in Sections 2.2.3 and 2.2.4. In a reverse reaction an adjoint particle can be either scattered or transformed into another type of adjoint particle. If during the reverse tracking an adjoint particle reaches the external surface without exceeding a user defined maximum energy (representing the maximum energy of the external source) its weight, final position, energy and direction are registered, and a forward particle equivalent to the primary adjoint particle is generated at the same starting position, with the same energy but as opposite direction and is tracked forward in the sensitive region of the geometry. During the forward tracking the different signals induced by the forward primary and its subsequent secondaries in the sensitive volume are computed. By this clear separation of the reverse and forward tracking phases it was possible to implement the RMC method such that only a few modifications are needed to an existing Geant4 application in order to adapt it for the use of the reverse simulation mode. The changes are needed only in the analysis phase at the end of the forward tracking where computed signals have to be multiplied by the final weights of the corresponding reverse tracks and then normalized to different user defined spectra and angular distribution representing the external source.

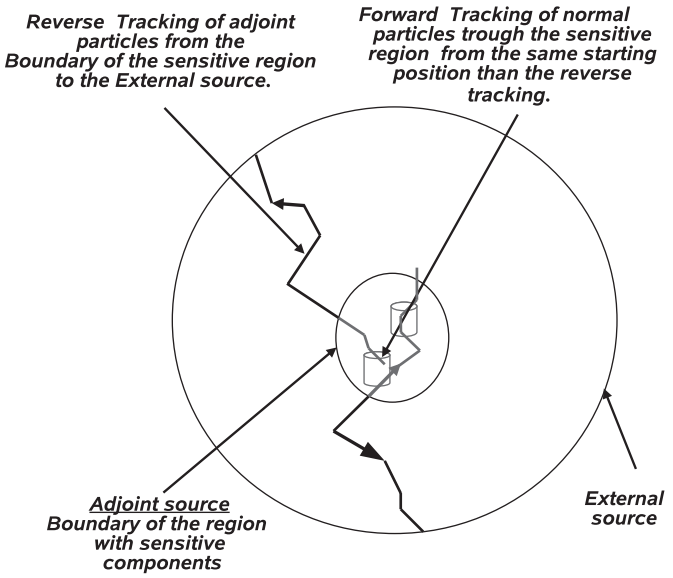

Fig. 2. Schematic view of the way we have implemented the reverse MC method in Geant4. See text for details.

3.2. Reverse physical processes

The reverse processes that have been implemented in Geant4 are the reverse e^-, proton, and ion ionization (continuous gain of energy and δe^- to projectile reverse reaction), the reverse e^- bremsstrahlung, the reverse Compton scattering, and the reverse photo-electric effect. They have been implemented based on the

corresponding processes of the G4 standard electromagnetic package [10].

3.2.1. Discrete reverse reactions

The reverse reactions are treated by considering the concept of adjoint differential cross-sections described in Section 2.2.1. For each process two different reactions are considered: the scattered projectile to projectile reaction and the product to projectile reaction. The differential cross-sections being not directly available in Geant4, they have been implemented for each process in form of an analytical formula where available, or of a numerical derivation of the forward cross-section provided in Geant4 over the energy of the product of the reaction. The adjoint cross-sections are obtained by the numerical integration of the differential cross-sections, over the energy of the forward primary projectile

$$\sigma^+(E) = \int_{E_{min}}^{E_{max}} \frac{d\sigma}{dE}(E' \to E)\frac{E}{E'}\, dE' \tag{17}$$

with the additional biasing factor E/E' explained in Section 2.2.4. The integration limits E_{min} and E_{max} represent, respectively, the minimum and maximum energy of the forward projectile that is a function of the energy E of the adjoint projectile equivalent to the forward product of the reaction.

The total adjoint macroscopic cross-section $\Sigma^+_{i,t}(E)$ for a specific type of particle i, and a given material is obtained by summing all the adjoint microscopic cross-sections over all types of reverse reactions and over all elements of the material, weighted with the element atomic densities. The total adjoint cross-section $\Sigma^+_{i,t}(E)$ and forward cross-sections $\Sigma_{i,t}(E)$ are computed and tabulated as a function of energy, for all types of particles and for all materials at the initial phase of the simulation. These tables are then used later to scale the adjoint cross-sections of all reverse reactions by the factor $\Sigma_{i,t}(E)/\Sigma^+_{i,t}(E)$. The reason for this scaling is explained in Section 2.2.3.

The energy E_1 of the secondary adjoint particle in a reverse reaction is sampled from the function

$$P(E \to E')_{E' < E_1} = \int_{E_{min}}^{E_1} \frac{d\sigma}{dE'}(E' \to E)\frac{E}{E'}\, dE' / \sigma^+(E) \tag{18}$$

that represents the probability to get a secondary adjoint particle with energy $E' < E_1$. The adjoint cross-sections and the probability functions are integrated numerically and tabulated as a function of energy in form of vectors and matrices. Once the energy of the secondary of a reverse reaction is obtained, its direction relative to the adjoint projectile is sampled as the direction of the products of the direct reaction relative to the forward projectile. The weight of the secondary adjoint particle is set to the weight of the primary adjoint particles multiplied by the factor $E_1\Sigma^+_{i,t}(E)/E\Sigma_{i,t}(E)$ with E and E_1 being, respectively, the energy of the adjoint projectile and secondary. The reasons of these corrections are explained in Sections 2.2.3 and 2.2.4.

3.2.2. Photo-electric effect

Compared to the other reverse electromagnetic processes that we have implemented in Geant4, the reverse photo-electric effect is treated differently as the energy of photo-electrons take discrete values. In the standard Geant4 photo-electric process the production of photo-electrons is calculated for a specific element from the following procedure:

- Starting from the K shell of the element the first shell having the binding energy B smaller than the energy of the photon is selected.
- The energy of the photo-electron is given by $E_e = E_\gamma - B$.
- The direction of the emitted photo-electron is taken from the Sauter–Gavrila distribution for K-shell [11] and is only function of the photo-electron energy.

Considering this and Eq. (17) we obtain for the adjoint macroscopic cross-section of the reverse photo-electric effect relative to an element in a material

$$\Sigma^+_{el}(E) = n_{el} \sum_{i, E < B_{i-1} - B_i} \sigma_{el}(E + B_i)\frac{E}{E + B_i} \tag{19}$$

with n_{el} the atomic> density of the element, $\sigma_{el}(E+B_i)$ the forward photo-electric microscopic cross-section, E the energy of the adjoint primary e^-, and B_i the binding energy of the ith shell. The macroscopic adjoint cross-section $\Sigma^+(E)$ for the reverse photo-electric effect relative to a material is then obtained by the summation of $\Sigma^+_{el}(E)$ over all elements of the material. The adjoint gamma emanating from the reverse photo-electric effect of an adjoint e^- interacting with a given material is generated as follows:

- An element of the material is randomly selected with the probability $\Sigma^+_{el}(E)/\Sigma^+(E)$.
- A shell of the selected element is selected randomly with probability

  $n_{el}\sigma_{el}(E+B_i)E/\Sigma^+_{el}(E)(E+B_i)$

  providing that the condition $E < B_{i-1} - B_i$ is fulfilled.
- The direction of the emitted adjoint gamma relative to the adjoint projectile e^- is selected as in the forward case from the Sauter–Gavrila distribution [11].
- The weights of the adjoint secondary are set following the same procedure used for other reverse discrete processes.

3.3. Continuous gain of energy

When tracking a charged particle backwards over one step a continuous gain of energy should be computed instead of the continuous loss computed during a forward simulation. The continuous loss of energy is computed in Geant4 in form of a mean energy loss and an additional fluctuation term. For a short step the mean energy loss dE over a step of length dx of a given particle type, in a given material is computed by

$$dE = dx S_{pow}(E) \tag{20}$$

where $S_{pow}(E) = dE/dx$ is the stopping power of the given particle in the given material. For a large step this approximation is no more valid and the mean energy loss is given by

$$dE = E - F_{R \to E}(F_{E \to R}(E) - dx) \tag{21}$$

where $F_{E \to R}(E)$ and $F_{R \to E}(R)$ are, respectively, the energy-to-range and range-to-energy functions tabulated during the initialization phase of Geant4 for each material and each particle type.

In the adjoint case the mean gain of energy over a small step is computed as in Eq. (20) while for a longer step length it is given by

$$dE = F_{R \to E}(F_{E \to R}(E) + dx) - E. \tag{22}$$

An additional loss fluctuation term is computed in Geant4 after the computation of the mean energy loss. To take into account this fluctuation in the adjoint simulation, we add to the mean energy gain the energy loss fluctuation obtained in the forward case at the energy $E = E_0 + dE_{mean}$ where dE_{mean} represents the mean energy gain and E_0 the energy before the step. Finally at the end of each tracking step the weight of an adjoint charged particle is corrected by the factor $S_{pow}(E_1)/S_{pow}(E_0)$ corresponding to the ratio between its stopping powers after and before the step. The need for this weight correction is explained in Section 2.2.6.

3.4. Multiple scattering

For simulating the reverse multiple scattering we use the same model as in the forward case. This approximation increases the discrepancy between the results of the adjoint simulation and forward simulation to a level of $\sim 10-15\%$.

4. Implementation of the RMC simulation mode into GRAS

The European Space Agency (ESA) is supporting the development and the use of the Geant4 Radiation Analysis for Space (GRAS) tool, aimed at the precise computation with Geant4 of space radiation effects on electronic components, solar panels,

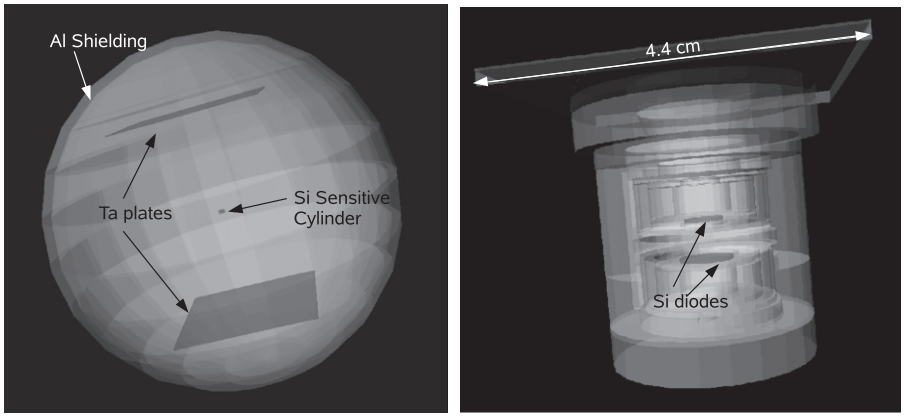

Fig. 3. The two types of geometry that we have used for testing the reverse Monte Carlo method implemented in Geant4. (left panel) The energy deposited is computed into a tiny silicon cylinder with 1 mm height and 1 mm radius, placed at the center of an aluminum spheric shell of 10 cm radius and 2 mm thickness. In addition there are two 0.5 mm tantalum plates placed above and below the cylinder. (right panel) For the second test case we used one detecting part of the ESAs Standard Radiation Environment Monitor (SREM) that is made of two aligned silicon diodes surrounded by different aluminum and tantalum shieldings [12].

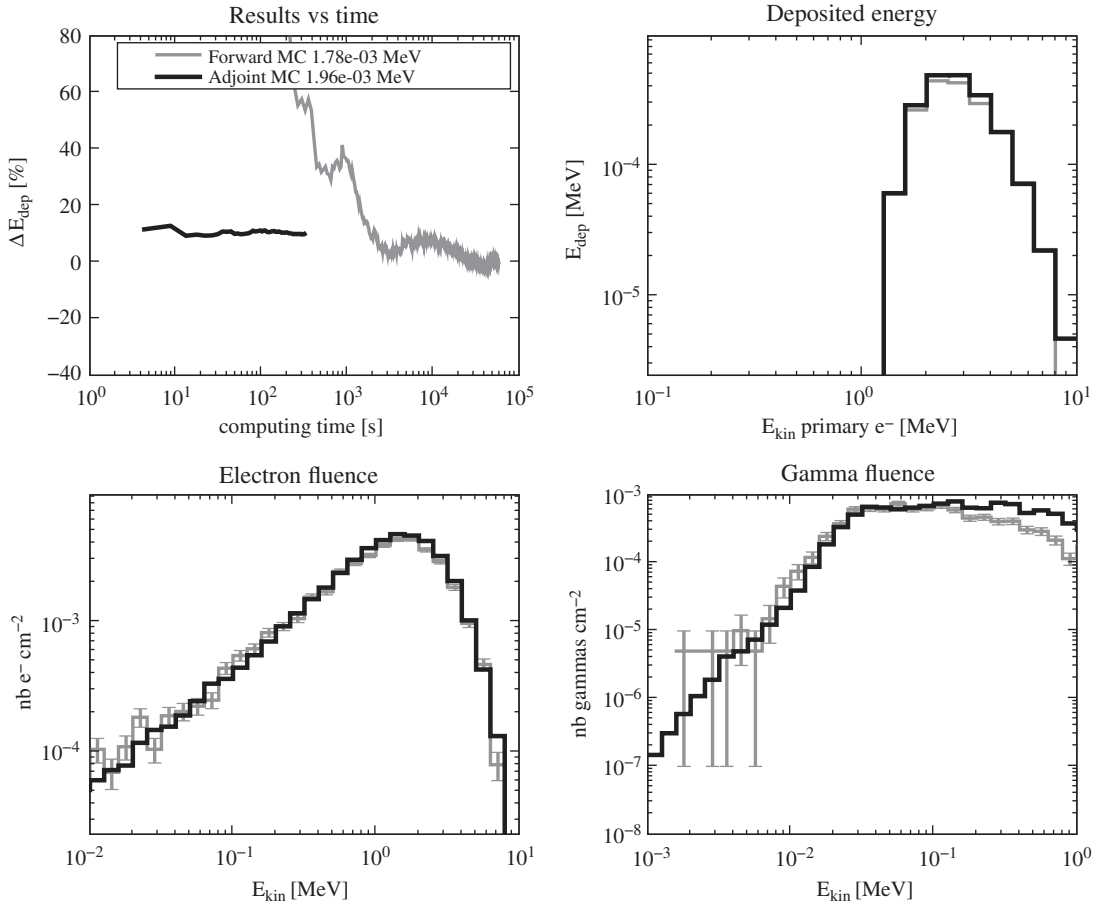

Fig. 4. Comparison of results obtained with Geant4 reverse (black) and forward (grey) MC simulations of the interaction of an external source of e^- with the geometry presented in the left panel of Fig. 3. The external source of e^- is isotropic, with an exponential spectrum $e^{-E/MeV}$ in the range [1 keV, 10 MeV], and a $1/cm^2$ omnidirectional fluence. (upper left panel) Energy deposited in the sensitive volume vs computing time. Plotted is the relative difference compared to the value obtained at the end of the forward simulation. (upper right panel) Energy deposited in the sensitive volume vs primary e^- energy. (lower left panel) Fluence of e^- entering the sensitive volume. (lower right panel) Fluence of γ entering the sensitive volume.

optical devices in complex payload and satellite geometry [5]. In GRAS a set of analysis modules (dose, fluence, LET spectrum, etc.) can be selected by the user through Geant4 interactive commands in order to rapidly setup a Geant4 simulation without the need of C++ coding. To make the GRAS code more attractive for space engineers who are often reluctant to use Monte Carlo codes because they are very time consuming, ESA has sponsored the extension of GRAS to use the Reverse MC mode implemented into Geant4. Because of the clear separation between the reverse and forward tracking phases in the implementation of the reverse MC method in Geant4 no modification of the existing analysis modules in GRAS was needed. It means that the definition of the GRAS analysis module for the forward and reverse MC modes is identical. The main modifications of the GRAS code required were in the analysis and histogram managers. For each scalar and 1D-histogram that is computed within GRAS during a forward simulation, a response matrix of the signal as a function of primary particle type and energy is computed during the adjoint simulation. At the end of an adjoint simulation these response matrices are then normalized to user-specified primary spectra which can be either exponential, power law, or defined by 1D-histograms. In this way only one simulation is needed to cover all the cases of primary external source in the space environment. At this time only isotropic external source can be considered but it could be extended in the future to non-isotropic cases.

5. Results and discussions

We have tested our implementation of the reverse MC method into Geant4 and its inclusion in GRAS with two test geometries presented in Fig. 3. The first test geometry, on the left panel, consists of a tiny silicon sensitive cylinder with 1 mm height and 1 mm radius placed at the center of an aluminum shielding spheric shell of 10 cm radius and 2 mm thickness. Two additional tantalum plates with 0.5 mm thickness are placed inside the shielding above and below the sensitive volume. We have computed, using both the adjoint and forward MC methods, the energy deposited in the sensitive cylinder as well as the flux of secondary particles entering this volume, for external isotropic source of electrons and protons. In all simulations the ionization, e^- bremsstrahlung, Compton scattering, photo-electric effect, and multiple scattering processes are applied.

In Fig. 4 all the results obtained for an external source of e^- with an exponential spectrum $e^{-E/\mathrm{MeV}}$, in the energy range [1 keV, 10 MeV], and with an omnidirectional fluence of $1/\mathrm{cm}^2$ are presented in black for the reverse MC mode and in grey for the forward MC mode. In the upper left panel the difference in percent of the computed energy deposited in the sensitive cylinder relative to the energy deposited obtained at the end of the forward simulation is plotted as a function of computing time. All computations presented here were done on an Intel Xeon quad core 2.4 GHz processor, by using only one core for each simulation

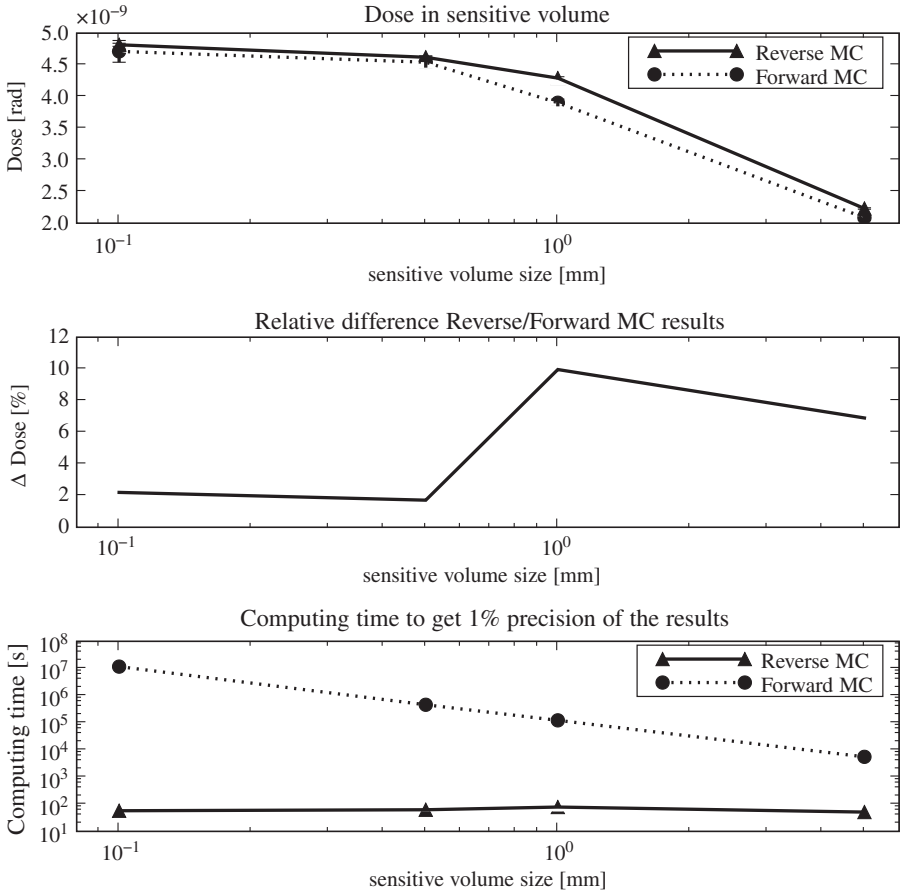

Fig. 5. Comparison of results obtained with Geant4 reverse (triangle) and forward (circles) MC simulations of the interaction of an external source of e^- with the geometry presented in the left panel of Fig. 3 and by considering different sizes of the sensitive volume. The size of the sensitive volume defines its height and radius. The external source of e^- is isotropic, with an exponential spectrum $e^{-E/\mathrm{MeV}}$ in the range [1 keV, 10 MeV], and a $1/\mathrm{cm}^2$ omnidirectional fluence. (upper panel) Computed dose in the sensitive volume. (mid panel) Relative difference in computed dose between reverse and forward MC simulation. (lower panel) Computing time needed to get 1% precision in the computed dose.

case. A $\sim 10\%$ discrepancy is observed between the deposited energies computed with the reverse and forward MC simulations. In the upper right panel of Fig. 4 the energy deposited is plotted as a function of the energy of the primary e^-. In the lower left and right panels the number of e^- and γ entering the sensitive cylinder is also plotted as a function of energy. The energy deposited vs primary and the secondary e^- spectrum obtained for the two simulations are in good agreement. A good agreement is also obtained for the flux of gamma at energy < 200 keV while at higher energy the discrepancy is increasing. The reason for these discrepancies between the forward and reverse Monte Carlo results will be discussed later on.

It is clear from the upper left panel of Fig. 4 that for this specific simulation case where the sensitive part is very small compared to the rest of the geometry the reverse MC method reaches precise results much more rapidly than the forward MC method. To quantify the rapidity of the different Monte Carlo methods to achieve a required precision of the results we use the figure of merit (FOM) for the energy deposited defined as

$$FOM = \frac{1}{R^2 T\ [\mathrm{min}]} \tag{23}$$

with R the relative precision of the computed deposited energy and T the computing time in minute needed to reach this precision. For the reverse and forward results presented in Fig. 4 we have FOMs of 7600 and 4.9, respectively. This means that the reverse MC method is approximately 1250 times more rapid than the forward MC method to reach the same level of precision in the computed results. In other words the reverse Monte Carlo method reaches 5%, 2% and 1% precision in approximately 3, 20 and 80 s computing time, respectively, while the forward Monte Carlo method get the same precisions after 1.36, 8.5 and 34.5 h, respectively.

We have also investigated how the size of the sensitive volume affects the reverse and forward Monte Carlo simulation results. Fig. 5 represents the Geant4 reverse and forward MC computed dose in the sensitive volume as a function of its size (radius and height of the sensitive cylinder). We can see from the upper and mid-panels that the same dependence of the computed dose on the size of the sensitive volume is obtained for the reverse and forward MC simulations and that a maximum relative difference of 10% is observed between the two simulation modes. In the lower panel it is shown that the time needed to get a 1% precision in the reverse simulation case does not change as a function of the size of the sensitive volume and is roughly 70–80 s for this particular geometry setup. On the contrary in the forward MC mode the computing time increases significantly when the size of the sensitive volume decreases and is several orders of magnitude higher than the computing time of the reverse MC simulation.

In Fig. 6 the results obtained with the first test case (see left panel of Fig. 3) for an external source of protons with a $1/E$ spectrum, an energy range of [1 keV, 200 MeV], and an omnidirectional fluence of $1/\mathrm{cm}^2$ are presented in the same way

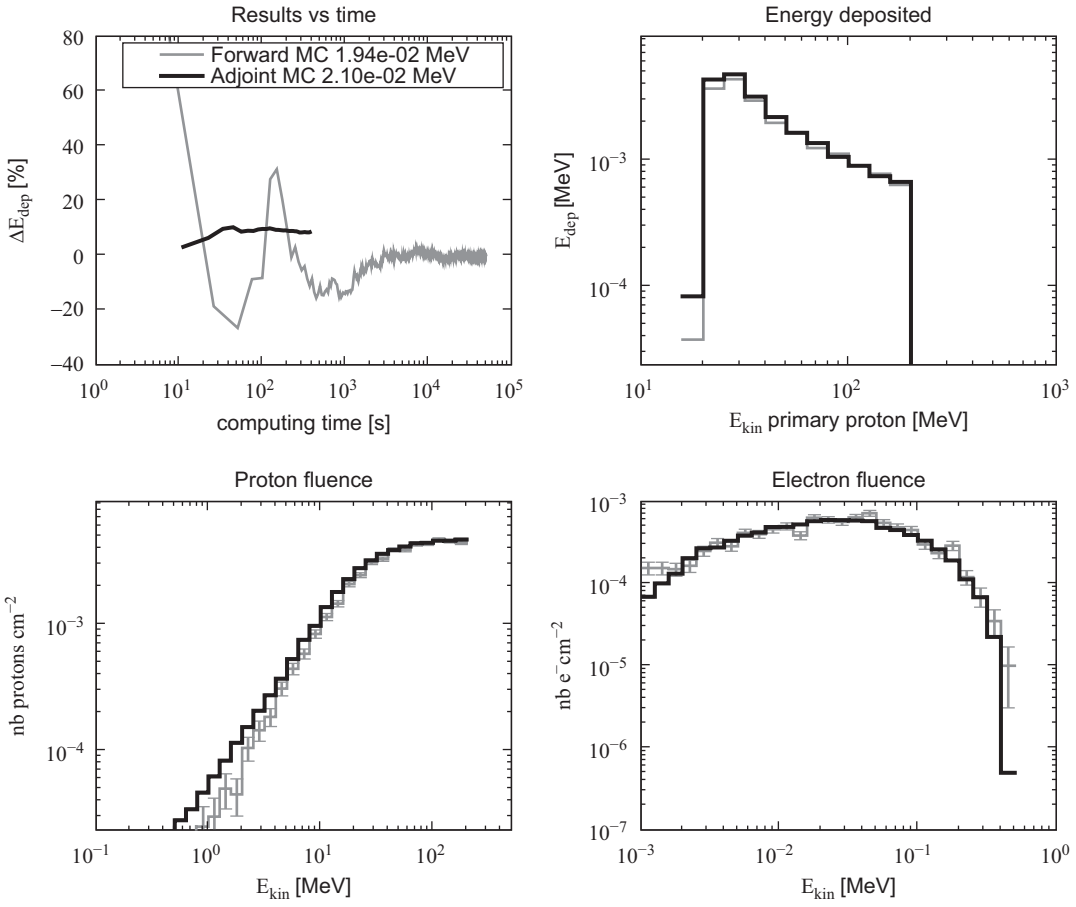

Fig. 6. Comparison of results obtained with Geant4 reverse (black) and forward (grey) MC simulations of the interaction of an external source of protons with the geometry presented in the left panel of Fig. 3. The external source of proton is isotropic, with a $1/E$ spectrum in the range [1 keV, 200 MeV] and a $1/\mathrm{cm}^2$ omnidirectional fluence. (upper left panel) Energy deposited in the sensitive volume vs computing time. Plotted is the relative difference compared to the value obtained at the end of the forward simulation. (upper right panel) Energy deposited in the sensitive volume vs primary proton energy. (lower left panel) Fluence of protons entering the sensitive volume. (lower right panel) Fluence of e^- entering the sensitive volume.

as in Fig. 4 with the exception that in the lower left and right panels the fluence of protons and e^- entering the sensitive volume are plotted, respectively.

The relative difference between the total energy deposited computed with the two methods is $\sim 8\%$. The energy deposited as a function of primary energy as well as the computed flux of proton and e^- entering the sensitive volume obtained with the two methods are in good agreement. The FOMs of the reverse and forward MC computations are 6450 and 5.7, respectively. It means that for the simulation case considered here the reverse MC method is approximately 1000 times more rapid than the forward MC method to get the same level of precision in the computed results.

For the second simulation case, we use the geometry represented in the right panel of Fig. 3. It corresponds to one detector of the ESAs Standard Radiation Environment Monitor (SREM), which consists of two silicon diodes placed in telescope alignment, and surrounded by different aluminum and tantalum shieldings. The plate at the top of the detector is 4.4 cm large [12]. We have computed with the reverse and forward MC methods the energy deposited in the smaller top diode as well as the flux of secondary particles entering this diode, for external isotropic sources of electrons and protons.

In Fig. 7 the results obtained for an external source of e^- with an exponential spectrum $e^{-E/\mathrm{MeV}}$, in an energy range [1 keV, 10 MeV], and with an omnidirectional fluence of $1/\mathrm{cm}^2$ are presented in the same way as in Fig. 4. The difference between the total deposited energy obtained with the reverse and forward MC simulation is 2–3%. A fairly good agreement is observed between the two simulation modes for the dependence of the energy deposited on the primary energy with more significant discrepancies at smaller energy. The agreement between the computed flux of entering e^- is rather good at all energies. The computed gamma fluxes are in very good agreement at energy smaller than 200 keV, while higher discrepancies are observed at higher energy. The FOMs of the reverse and forward MC computation are 200 and 2.7, respectively, for this simulation. It means that, although the size of the sensitive diode is not very small compared to the whole geometry, the reverse MC method is still 70 times more rapid than the forward MC method for this simulation case.

In Fig. 8 the results obtained with the second simulation test case (see right panel of Fig. 3) for an external source of protons with a power law spectrum E^{-2}, in an energy range [100 keV, 200 MeV], and with an omnidirectional fluence of $1/\mathrm{cm}^2$ are presented in the same way as in Fig. 6. The difference between the total deposited energy obtained with the reverse and forward MC simulation is 20%. A good agreement is observed between the energy deposited vs primary energy. The agreement between the computed flux of entering proton is very good at all energy. The computed flux of secondary electrons is systematically higher for the reverse MC method as compared to the forward MC method. The FOMs of the reverse and forward MC computation are 1000 and 4, respectively. This means that for this simulation case the reverse MC method is still 250 more rapid than the forward MC method.

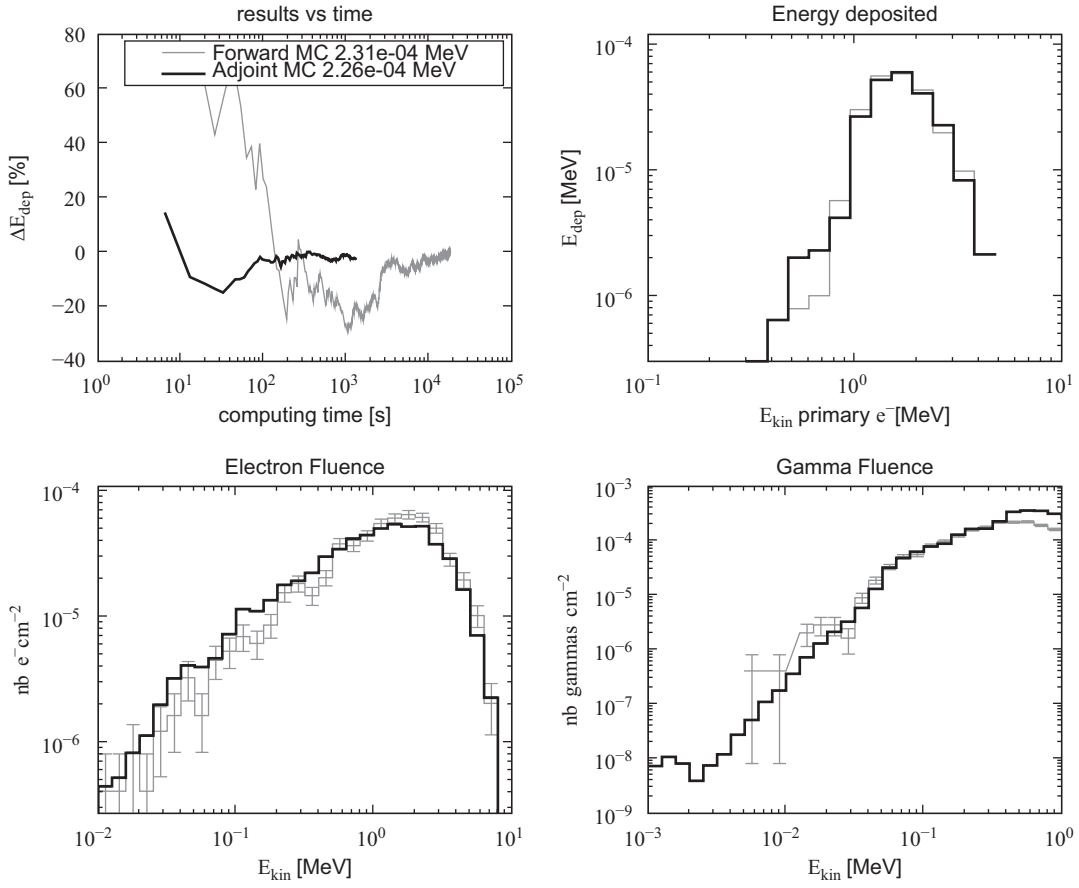

Fig. 7. Comparison of results obtained with Geant4 reverse (black) and forward (grey) MC simulations of the interaction of an external source of e^- with the geometry presented in the right panel of Fig. 3. The external source of e^- is isotropic, with an exponential spectrum $e^{-E/\mathrm{MeV}}$ in the range [1 keV, 10 MeV] and a $1/\mathrm{cm}^2$ omnidirectional fluence. (upper left panel) Energy deposited in the sensitive volume vs computing time. Plotted is the relative difference compared to the value obtained at the end of the forward simulation. (upper right panel) Energy deposited in the sensitive volume vs primary e^- energy. (lower left panel) Fluence of e^- entering the sensitive volume. (lower right panel) Fluence of γ entering the sensitive volume.

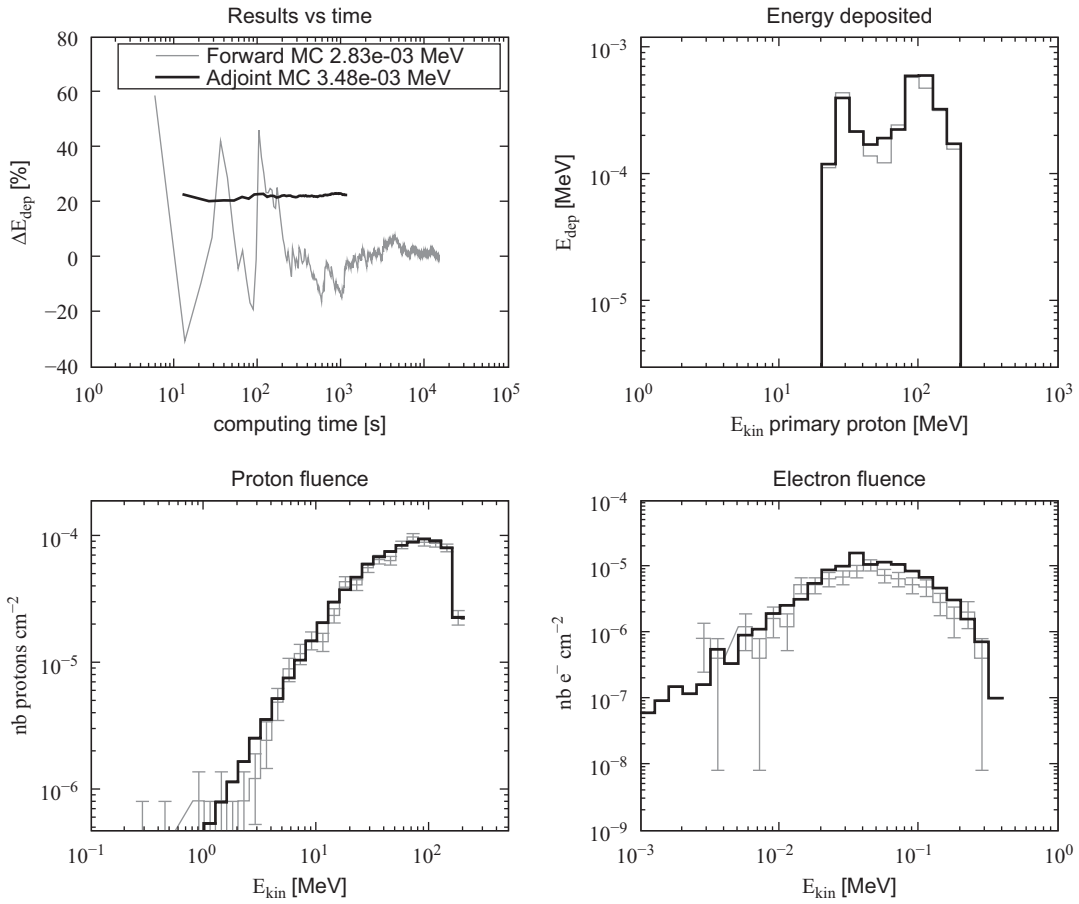

Fig. 8. Comparison of results obtained with Geant4 reverse (black) and forward (grey) MC simulations of the interaction of an external source of protons with the geometry presented in the right panel of Fig. 3. The external source of proton is isotropic, with a $1/E^2$ spectrum in the range [1 keV, 200 MeV] and a $1/cm^2$ omnidirectional fluence. (upper left panel) Energy deposited in the sensitive volume vs computing time. Plotted is the relative difference compared to the value obtained at the end of the forward simulation. (upper right panel) Energy deposited in the sensitive volume vs primary proton energy. (lower left panel) Fluence of protons entering the sensitive volume. (lower right panel) Fluence of e^- entering the sensitive volume.

While the results of the adjoint MC method are in general in good agreement with the results obtained with the forward MC method, some discrepancies are observed. An important source of these discrepancies is the fact that we have used for the reverse multiple scattering the same model as in the forward mode of Geant4. In this approximation the mean angular deviation is computed systematically at energy smaller than in the forward case as the multiple scattering effect is computed at the energy that a particle has at the beginning of the reverse step, corresponding to the end of the forward step. The systematic difference in secondary e^- fluxes in the lower right panel of Fig. 8 is mainly due to this approximation.

Another source of discrepancy is due to the fact that the differential cross-section used in the reverse bremsstrahlung process is different from the one used in the forward bremsstrahlung as modeled in the Geant4 standard electromagnetic package. This difference is the source of a higher flux of >100 keV gamma in the reverse simulation compared to the forward simulation as can be seen in the lower right panels of Figs. 4 and 7. The differential cross-section used in the reverse bremsstrahlung model is obtained by numerical derivation of the direct cross-section provided by the forward model over the energy of the secondary γ. This would be a correct procedure if the distribution of secondaries in the forward bremsstrahlung model would be sampled from this differential cross-section. Unfortunately it is not the case as in the Geant4 electromagnetic standard package independent parameterizations are used for the cross-sections and the sampling of secondary for the bremsstrahlung process. It means that in the forward model if one integrates the effective differential cross-section used for the production of bremsstrahlung gammas it would not be the same as the parameterized cross-section. In the future we plan to correct this problem by using an extra weight correction factor after the occurrence of a reverse bremsstrahlung. This weight factor should be the ratio between the differential CS used in the adjoint simulation and the one effectively used in the forward bremsstrahlung model. For this purpose we are investigating the feasibility to use the differential cross-section in the implementation of the PENELOPE electromagnetic models in Geant4.

It has also to be mentioned that in some rare cases an adjoint track may get a much too high weight when reaching the external source. While this does not happen often it may significantly corrupt the simulation results. The reason of this high weight is the occurrence at low electron and gamma energy of both the photo-electric and bremsstrahlung processes within the same adjoint tracks. Unfortunately we still need further investigations to remove this problem at the level of physical processes. However, this weight can be removed in the analysis part of the code by adding a test on the adjoint weight after the adjoint tracking phase. This has been done for the simulation results that we have presented here, and equivalent correction code is available to the users in the provided examples.

6. Conclusion

We have successfully implemented the reverse/adjoint Monte Carlo method into the Geant4 toolkit and added it to the GRAS tool for electron, proton, and ion electromagnetic processes. By considering two different simulation cases we have shown that the Geant4 reverse Monte Carlo mode provides results in fairly good agreement with the forward MC results and within much less computing time than the forward MC mode. In the future we plane to reduce the $\sim 10\%$ discrepancies between the reverse and forward MC results by improving the models for the reverse multiple scattering and the reverse bremsstrahlung processes. We are also considering the possibility to extend the reverse MC mode in Geant4 to some hadronic processes as for example low energy neutron elastic and inelastic scattering.

Acknowledgments

This work has been performed under the ESA/ESTEC Contract 21435/08/NL/AT. We thank M. Asai, M. Verderi, J. Apostolakis, G. Cosmo, and V. Ivanchenko for fruitful discussions regarding the design to the Geant4 kernel and identifying some limitations of its first implementation. We thank W. Hajdas to have provided us with the description of the SREM geometry. We thank also P. Nieminen for having carefully read this manuscript. Finally we thank the editor and the referees for their constructive comments during the review of this paper.

References

[1] M.H. Kalos, Nucl. Sci. Eng. 33 (1968) 284.
[2] B. Eriksson, C. Johansson, M. Leimdorfer, Nucl. Sci. Eng. 37 (1969) 410.
[3] T. Jordan, Space system analysis using the novice code system, in: First European Conference on Radiation and its Effects on Devices and Systems, RADECS91, 1991, pp. 312–316.
[4] J. Allison, K.K. Amako, J. Apostolakis, H. Araujo, P. Dubois, M. Asai, G. Barrand, R. Capra, S. Chauvie, R. Chytracek, G. Cirrone, G. Cooperman, G. Cosmo G. Cuttone, G. Daquino, M. Donszelmann, M. Dressel, G. Folger, F. Foppiano J. Generowicz, V. Grichine, S. Guatelli, P. Gumplinger, A. Heikkinen I. Hrivnacova, A. Howard, S. Incerti, V. Ivanchenko, T. Johnson, F. Jones T. Koi, R. Kokoulin, M. Kossov, H. Kurashige, V. Lara, S. Larsson, F. Lei, O. Link, F. Longo, M. Maire, A. Mantero, B. Mascialino, I. McLaren, P. Lorenzo K. Minamimoto, K. Murakami, P. Nieminen, L. Pandola, S. Parlati, L. Peralta, J. Perl, A. Pfeiffer, M. Pia, A. Ribon, P. Rodrigues, G. Russo, S. Sadilov, G. Santin, T. Sasaki, D. Smith, N. Starkov, S. Tanaka, E. Tcherniaev, B. Tome, A. Trindade, P. Truscott, L. Urban, M. Verderi, A. Walkden, J. Wellisch, D. Williams D. Wright, H. Yoshida, IEEE Trans. Nucl. Sci. NS-51 (1) (2006) 270.
[5] G. Santin, V. Ivantchenko, H. Evans, P. Nieminen, E. Daly, IEEE Trans. Nucl. Sci. NS-52 (1) (2005) 2294.
[6] J.E. Hoogenboom, Nucl. Sci. Eng. 79 (1981) 357.
[7] J.E. Hoogenboom, Nucl. Sci. Eng. 141 (2003) 99.
[8] L.B. Levitt, J. Spanier, Nucl. Sci. Eng. 37 (1969) 278.
[9] T.M. Jordan, An adjoint charged particle transport method, E.m.p. Consultants Report, 1976.
[10] J. Apostolakis, M. Asai, A. Bogdanov, H. Burkhardt, G. Cosmo, S. Elles, G. Folger, V. Grichine, P. Gumplinger, A. Heikkinen, I. Hrivnacova, V. Ivanchenko, J. Jacquemier, T. Koi, R. Kokoulin, M. Kossov, H. Kurashige, I. McLaren, O. Link, M. Maire, W. Pokorski, T. Sasaki, N. Starkov, L. Urban, D. Wright, Radiat. Phys. Chem. 78 (10) (2009) 859.
[11] M. Gravila, Phys. Rev. 113 (1959) 514.
[12] W. Hajdas, P. Buehler, C. Eggel, P. Favre, A. Mchedlishvili, A. Zehnder, Astron. Astrophys. 411 (2003) 43.